Photon Jet Search for Axion-like Particles: Trigger Study

REU Program at Columbia University - Nevis Labs

Sophia Garcia

UC Irvine

August 1, 2025

Abstract

This report investigates the efficiency of diphoton triggers within the ATLAS Experiment at CERN, specifically in the context of searching for Axion-Like Particles (ALPs) produced from the decay of a heavy scalar particle ($X \to 4\gamma$). The study addresses the experimental challenge posed by highly collimated photons from ALP decays, which can mimic single-photon signatures and impact trigger performance.

Using Monte Carlo simulations across various ALP masses, we analyze the transverse momentum distributions and trigger efficiencies for loose, medium, and tight photon identification criteria. Our findings indicate that while loose triggers maintain high efficiency, the efficiency of medium and tight triggers significantly degrades with increasing ALP mass. This degradation is attributed to the broadening of photon shower shape variables (specifically w_{stot}, ΔE_s, and E_{ratio}) at higher ALP masses, signifying less collimated photon pairs. The results highlight the need for optimized trigger strategies and advanced reconstruction techniques to enhance sensitivity to these unique signatures in future searches for Beyond Standard Model phenomena.

Contents

1 Introduction

1.1 Standard Model

The Standard Model[1] is a well-established theory of particle physics, finalized in the 1970s, that describes three of the four fundamental forces (electromagnetic, weak, and strong interactions) and classifies all currently known elementary particles. While it remains the most successful framework for describing fundamental interactions, the Standard Model has known limitations: it does not incorporate gravity, fails to account for the presence of dark matter, and cannot explain the observed matter–antimatter asymmetry in the universe. Notable experimental confirmations and additions to the model include the discovery of the top quark (1995), the tau neutrino (2000), and the Higgs boson (2013).

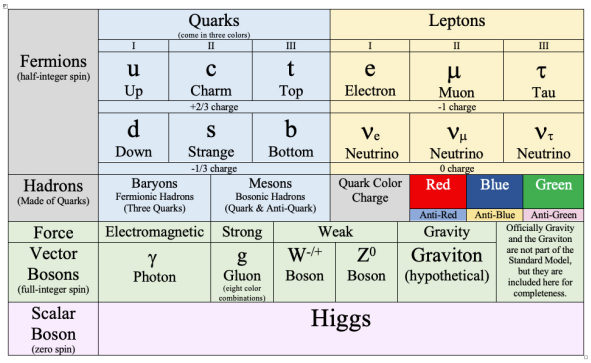

Figure 1: *The Standard Model of particle physics.*

Matter is composed of fundamental particles known as fermions, which are responsible for baryonic mass. Fermions are divided into three generations, ordered from lightest to heaviest. The first generation forms most of the visible matter in the universe, while the heavier generations are unstable and decay into lighter ones. Fermions include two categories: quarks and leptons. Quarks interact via strong nuclear force and combine to form hadrons, such as protons and neutrons. Leptons, which include electrons and neutrinos, do not participate in the strong interaction.

Force-carrying particles, known as gauge bosons, mediate the fundamental interactions between fermions. Gluons carry the strong force, photons mediate the electromagnetic force, and W and Z bosons are responsible for the weak interaction. The Higgs boson, discovered in 2013, is a scalar boson responsible for mass generation through the Yukawa interaction.

1.2 The Strong Charge-Parity Problem

The weak interaction, mediated by the exchange of integer-spin force-carrying bosons (W^+, W^-, and Z), governs phenomena such as radioactive decay. This fundamental force is distinct for its violation of parity symmetry (P), which involves spatial inversion, and charge conjugation symmetry (C), the transformation of particles into their antiparticles. Although it was initially theorized that the combined charge-parity symmetry (CP) might be conserved in weak interactions, subsequent experiments conclusively demonstrated that CP-symmetry is also violated in certain weak processes. QCD allows CP violation, and predicts it in both weak and strong interactions, however, the CP violation coefficient in strong interactions is close to zero. This experimental observation leads to a significant theoretical puzzle: while the Standard Model predicts a similar CP-violation within the strong interaction, why has none ever been empirically observed? This discrepancy is known as the Strong CP Problem.

1.2.1 Axion and Axion-Like Particles

A prominent proposed solution to the Strong CP Problem involves extending the Standard Model to include a hypothetical particle called the QCD axion[2]. Axions are light, neutral, and weakly interacting particles that naturally suppress CP-violation in strong interactions. A broader category of such particles, known as axion-like particles (ALPs), is the main focus of this project. We hypothesize that in the decay of a heavy scalar particle, such as a Higgs-like boson, two ALPs are produced via the decay channel. In the energy regime probed by the LHC (100 MeV to 10 GeV), ALPs are expected to be very light. Due to kinematic laws, the ALPs will most likely decay into two photons or very light leptons, which occurs because ALPs need its decay products to be half of its original rest mass.

2 Instrumentation

2.1 ATLAS Detector

The ATLAS Detector[3] is a large multilayered instrument that detects many different fundamental particles. It is one of the two general purpose detectors at the Large Hadron Collider (LHC) at CERN. ATLAS is designed to accommodate large energy scales, and has a cylindrical geometry, measuring 44 meters in length and 25 meters in diameter. Its subdetectors are arranged in concentric layers and include tracking detectors, calorimeters, and muon spectrometers. ATLAS is designed to detect the signatures of a wide range of processes, including Higgs boson product, supersymmetric particles, and other evidence of particles beyond the Standard Model.

2.2 Liquid Argon Calorimeter

The Liquid Argon (LAr) calorimeter[4] is a crucial subsystem of ATLAS, designed to measure the energy and position of electrons, photons, and Hadronic particles with high precision. It consists of three main components: the electromagnetic (EM) calorimeter, the Hadronic end-cap (HEC), and the forward calorimeter (FCAL), all housed in large cryostats. In the context of this study, the LAr Calorimeter is particularly valuable for identifying photon-rich final states with high granularity and longitudinal segmentation. The fine shower shape information and precise timing allow advanced reconstruction algorithms and machine learning models to improve signal identification and background suppression in rare event searches.

2.3 ATLAS Trigger System

The ATLAS trigger system[5] is a critical component of the detector's data acquisition pipeline, responsible for reducing the immense bunch crossing rate of 40 MHz (bunch crossings every $25ns$) to a manageable data storage rate of approximately 1 kHz. This reduction is essential for selecting the most interesting physics events while discarding the vast majority of background. The trigger system operates in two levels: hardware-based Level 1 (L1), and software based High-Level Trigger (HLT).

The Level 1 Trigger is implemented in custom electronics and uses coarse detector information from the calorimeters and muon systems to make a decision within a fixed latency of 2.5 microseconds. It reduces the event rate from 40 MHz to about 100 kHz. In the electromagnetic calorimeter, L1 trigger towers combine calorimeter cells into coarser segments, typically with granularity ($\Delta\eta$, $\Delta\phi$) to identify regions with high energy deposits characteristic of electromagnetic objects like photons and electrons. The L1 system also includes a central trigger processor

(CTP), which applies logic conditions (such as requiring multiple objects above threshold) and handles dead-time control and prescaling.

Events passing L1 are sent to the (HLT), which is a fully software-based system running on a computing farm. The HLT uses full detector granularity and precision to refine the event selection. It reconstructs the physics objects such as electrons, muons, photons, jets, and missing transverse momentum using algorithms that are similar to the offline reconstruction but optimized for speed. The HLT reduces the rate further (from 100 to 1 kHz) which ensures that only events are written to disk for analysis. The HLT also performs regional reconstruction, meaning that only the regions of the detector flagged by L1 are processed initially, allowing for faster event handling. In cases where more information is needed, the reconstruction can expand to the full event. Machine learning techniques have been integrated into the HLT framework to improve object identification and pile-up rejection. The trigger system must balance efficiency and selectivity, especially for the search for rare signals. Thus, special attention is given to developing trigger menus that are sensitive to such topologies. The terms "loose," "medium," and "tight" refer to predefined sets of selection criteria used in photon identification or trigger requirements. These categories represent increasing levels of strictness, with "loose" applying the least restrictive conditions. Photon-based triggers also typically impose minimum transverse energy p_T thresholds. These thresholds help maintain high signal efficiency while reducing background contamination.

3 Photon-jet Search for Axion-like Particles

Axion-like Particles[6] (ALPs) are hypothetical pseudoscalar particles that arise in many extensions of the Standard Model, including those addressing the Strong CP Problem, dark matter, and string theory compactification. Unlike the QCD axion, their mass and coupling strength are treated as independent parameters. This study focuses on ALPs produced via the decay of a heavy Standard Model scalar, such as the Higgs boson, through the channel:

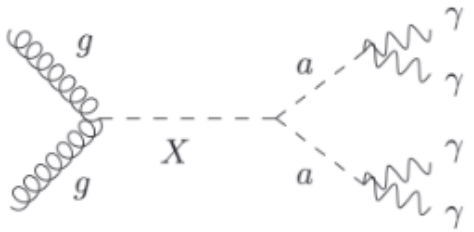

Figure 2: *($X \to \gamma\gamma$ Feynman Diagram)*

This decay chain leads to a distinctive final state featuring four photons. According to kinematics, an ALP will predominantly decay into two photons or light leptons, because the decay products must carry away half the parent particle's rest mass. Conservation of momentum further implies that these photons will be highly collimated.

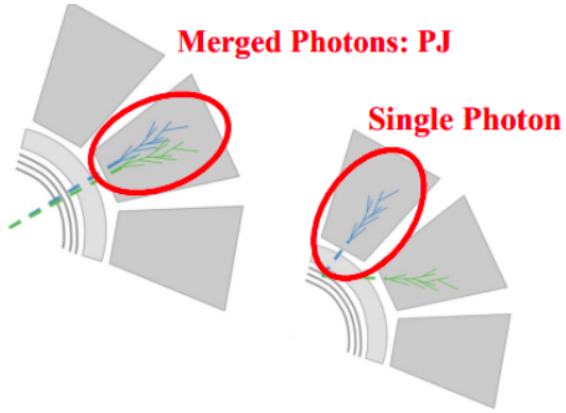

Figure 3: *(Depiction of Photon jets at Cell level)*

This creates a major experimental challenge: if the decay photons are emitted at a small angle, their energy deposits may overlap in the detector and mimic the signal of a single photon (see Figure 3). Compounding this difficulty, the background processes in LHC collisions naturally contain many photons, increasing the chance of misidentification. Efforts to use a machine-learning algorithm to correctly identify these characteristics is our main goal here. However, the training of such a model requires clean data for optimal learning. Due to the nature of these characteristics, it is in our best interest to study our current trigger strategies. An important goal is to evaluate how tighter photon triggers affects the sensitivity to collimated photon pairs. These definitions may inadvertently suppress signal efficiency if merged photon pairs fail to meet isolation or shower shape criteria.

In our trigger study, we analyzed five different Monte Carlo samples. The first is a $H \to \gamma\gamma$ sample, which serves as a baseline for comparison with the other datasets. This sample was selected because of its clean final state, its similarity in final-state photon kinematics, and well-understood trigger performance[7]. As illustrated below, it involves a simple decay into two photons:

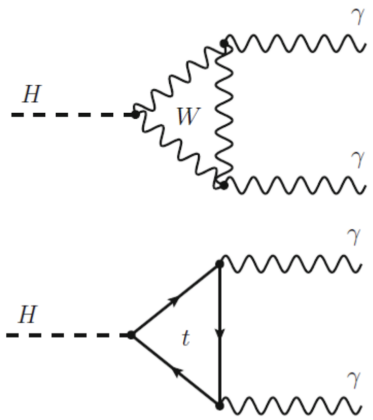

Figure 4: *Feynman diagram for the process $H \to \gamma\gamma$.*

This decay topology is similar to that of our $X \to \gamma\gamma$ search. To explore the effect of ALP mass on photon merging and trigger efficiency, we analyzed four additional $X \to aa$ Monte Carlo samples, with the ALP decaying to two collimated photons in each case. The samples span a range of increasing Scalar and ALP masses:

- 125 GeV$X \to$ 0.1GeV ALP
- 125 GeV$X \to$ 0.5GeV ALP

- 800 GeV$X \rightarrow$ 1.0GeV ALP
- 800 GeV$X \rightarrow$ 2.5GeV ALP

These samples were selected to study how increasing ALP mass impacts the angular separation of decay photons and, consequently, the detector response and trigger selection.

3.1 Identification and Event Selection

To ensure an accurate analysis of trigger efficiencies, we first apply a series of selection cuts to the data. A central aspect of our methodology is the reliable classification of events, which begins with filtering on the "Loose Identification" (Loose I.D.) variable. This variable corresponds to a predefined set of photon identification criteria and helps isolate events with well-reconstructed photons before evaluating trigger performance. In addition, we apply a "cleaning" requirement to reject calorimeter cells in the Liquid Argon (LAr) Calorimeter that may be affected by noise or other irregularities[8]. This step ensures that only high-quality, low-noise events are included in the analysis. Our study focuses exclusively on di-photon triggers. For this reason, we place particular emphasis on the subleading photon in each event, as it is more likely to fall below the trigger threshold and thus more often determines whether the event passes or fails the trigger. Here, the leading photon refers to the one with the highest p_T, while the subleading photon is the second-highest in p_T. Another consideration are the different p_T thresholds, such as 2G50 (requiring two photons with $p_T > 50$ GeV each), which offer different trade-offs between purity and acceptance. To account for this, we require events to contain at least two photons, each passing loose identification, clean cell identification, and transverse momentum thresholds of $p_T > 20$ GeV. These cuts are ideal to ensure a fair, unbiased, and reliable analysis of the trigger performance[6].

3.1.1 Kinematic Distributions

For the signal samples, it is standard practice to examine the transverse momentum (p_T) of both the leading and sub-leading photons in each event. This is particularly important for later studies of trigger efficiency as a function of photon p_T binning.

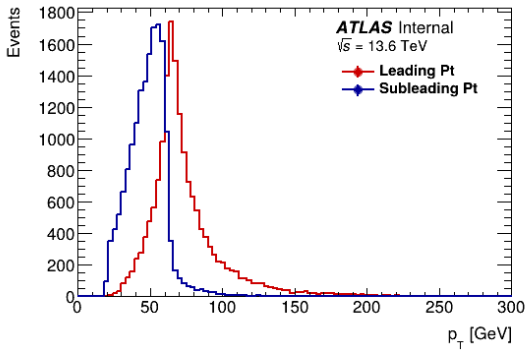

Figure 5: *Transverse momentum distribution of photons in the $H \rightarrow \gamma\gamma$ sample.*

As expected, the $H \rightarrow \gamma\gamma$ sample exhibits a peak in the leading photon p_T applied on medium around half the Higgs boson mass, consistent with the kinematics of a two-body decay[7].

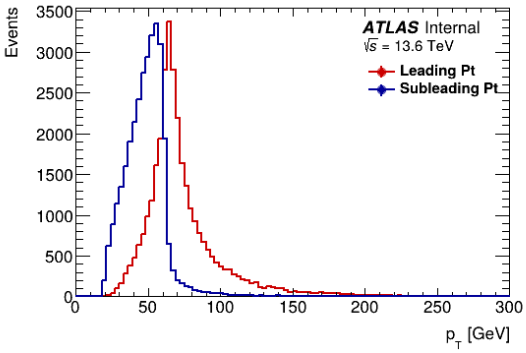

(a) 125 GeV $X \to 0.1$ GeV ALP

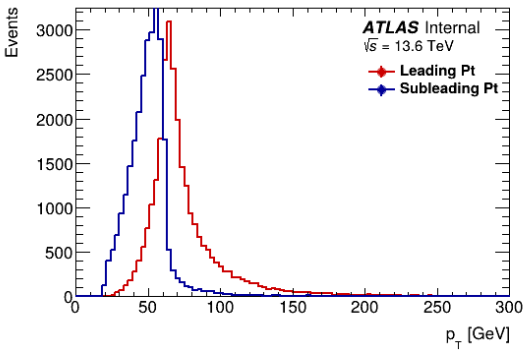

(b) 125 GeV $X \to 0.5$ GeV ALP

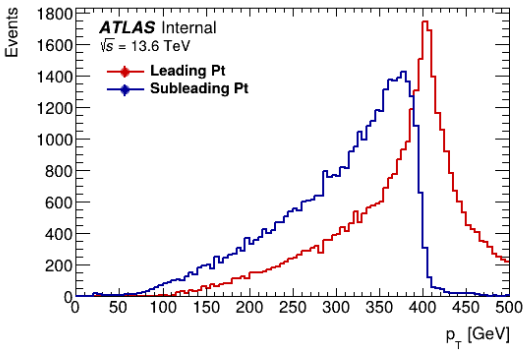

(c) 800 GeV $X \to 1.0$ GeV ALP

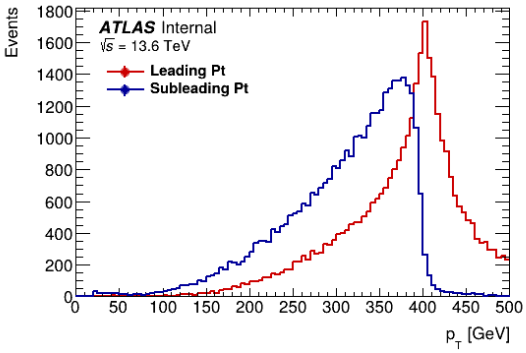

(d) 800 GeV $X \to 2.5$ GeV ALP

Figure 6: *Photon p_T distributions for ALP benchmark samples grouped by X mass: 125 GeV (top) and 800 GeV (bottom).*

Overall, the transverse momentum (p_T) distributions of the signal samples are consistent with expectations. The distributions peak around 62 GeV for the 125 GeV scalar mass samples and around 400 GeV for the 800 GeV scalar mass samples, aligning well with the behavior observed in the $H \to \gamma\gamma$ sample and consistent with two-body decay kinematics.

3.2 Trigger Analysis

We measured the trigger efficiency of a diphoton trigger as a function of the transverse momentum (p_T) of the subleading photon. The analysis was performed on the selected dataset described in the previous section. For each event containing a photon pair, we applied selection criteria requiring both photons to pass loose ID and cleaning cuts. We then used the TEfficiency class from ROOT to compute the trigger efficiency as:

$$\epsilon(p_T) = \frac{N_{\text{trigger}}}{N_{\text{total}}}$$

where N_{trigger} is the number of events satisfying both the determined cuts and the trigger, and N_{total} is the total number of events passing only the cuts.

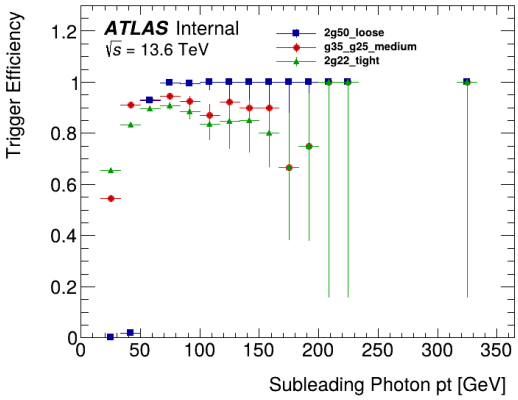

Figure 7: *Trigger Efficiency as a Function of p_T for the $H \to \gamma\gamma$ sample.*

Figure 7 presents the trigger efficiency curves for three different triggers: 2G50 loose, G25G35 medium, and 2G22 tight, which are plotted as a function of the p_T of the sub-leading photon in the $H \to \gamma\gamma$ sample. It illustrates a typical trigger efficiency "turn-on curve" for the $H \to \gamma\gamma$ sample. The term "turn-on curve" describes the rapid increase in trigger efficiency as the photon (p_T) crosses the trigger threshold. A well-behaved turn-on curve reaches a plateau near unity and maintains a stable efficiency beyond the threshold, a characteristic clearly demonstrated in this figure.

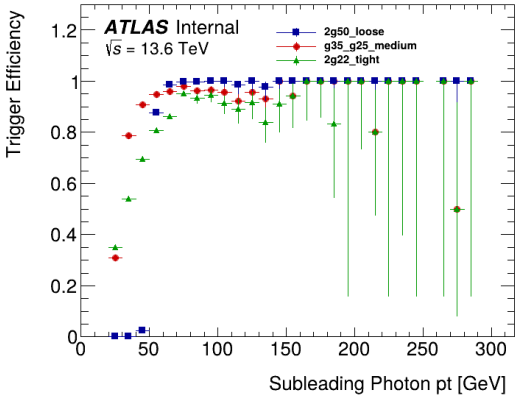

(a) *125 GeV $X \to 0.1$ GeV ALP*

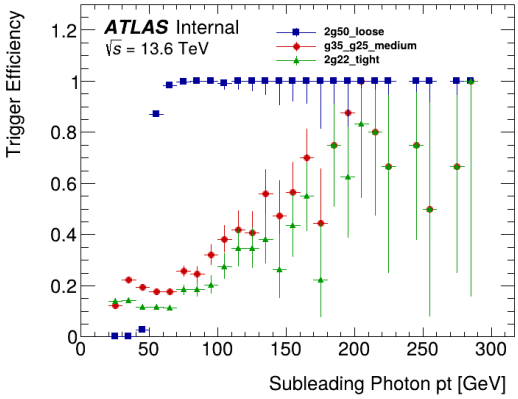

(b) *125 GeV $X \to 0.5$ GeV ALP*

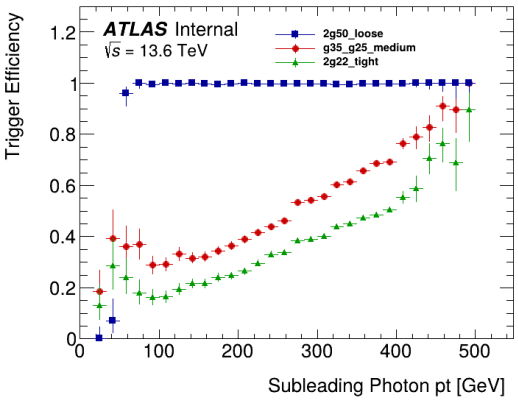

(a) *800 GeV $X \to 1.0$ GeV ALP*

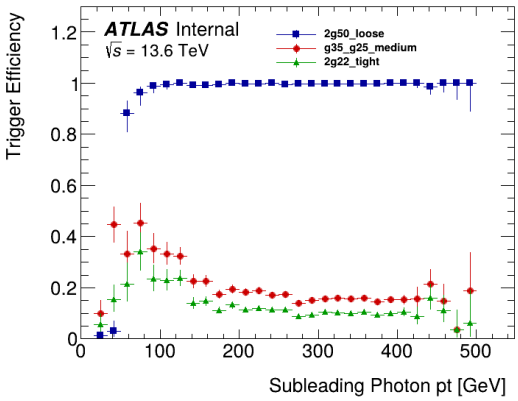

(b) *800 GeV $X \to 2.5$ GeV ALP*

Figure 9: *Trigger Efficiencies as a function of p_T for ALP benchmark samples grouped by X mass: 125 GeV (top) and 800 GeV (bottom).*

As illustrated in Figure 9 above, the analysis begins with the lowest ALP mass sample, 125 GeV$X \to$ 0.1GeV ALP, progressing to the highest mass. The 0.1 GeV ALP sample exhibits strong trigger efficiencies, with the three triggers plateauing around 100%, 95%, and 90% respectively. However, as the ALP mass increases, the trigger efficiencies for the medium and tight working points degrade significantly. Notably, the 2.5 GeV ALP sample shows markedly reduced efficiencies for both medium and tight triggers. In contrast, the loose trigger efficiency remains largely stable across all ALP masses. This behavior suggests two key points: first, that medium and tight triggers rely on a particular variable or set of variables affecting trigger acceptance, and second, that the signal events degrade with respect to this variable as the ALP mass increases.

Signal	**2g50 Loose**	**g25 g35 Medium**	**2g22 Tight**
$H \to \gamma\gamma$	45.04%	87.27%	83.90%
125 GeV $X \to$ 0.1 GeV ALP	43.08%	85.26%	69.80%
125 GeV $X \to$ 0.5 GeV ALP	46.80%	19.18%	12.79%
800 GeV $X \to$ 1.0 GeV ALP	99.51%	56.36%	40.50%
800 GeV $X \to$ 2.5 GeV ALP	99.26%	16.36%	10.56%

Table 1: *Photon Trigger Efficiency for each signal under the Loose, Medium, and Tight.*

Table 1 presents the efficiency as the ratio $\frac{N_{trigger}}{N_{total}}$ for each signal and trigger configuration. The general trend is that the loose trigger yields the highest efficiencies, the medium trigger falls in the middle, and the tight trigger exhibits the lowest efficiencies. However, for the $H \to \gamma\gamma$ and 125 GeV$X \to$ 0.1GeV ALP samples, the loose trigger efficiency is lower than that of the medium trigger. This behavior arises from differences in the p_T thresholds between the 2g50 (loose) and g25-g35 (medium) triggers. Additionally, the trigger efficiency results vary significantly with the ALP mass. As shown, for higher-mass samples, the efficiencies for the medium and tight triggers decrease substantially and remain at low values. This decline was anticipated for the tight trigger, given its more stringent selection criteria and the atypical, collimated nature of photons in our signals.

3.3 Shower Shape Variables

To understand the observed behavior of the medium and tight photon identification trigger efficiencies, we examined the dependence of several photon shower shape variables on the ALP mass and photon p_T. These variables characterize the spatial development of electromagnetic showers within the electromagnetic calorimeter (EMCal). These variables are particularly important because they are used as criteria that events must satisfy to pass certain triggers (like tight and medium). Therefore, such analysis provides insight into how the shower characteristics vary with the underlying ALP mass properties and influences trigger performance.

Key variables include:

- $w_{\mathbf{stot}}$ — the width of the shower in the strip layer (first EM layer), computed over the full window (20 strips). This helps resolve close-by energy peaks from overlapping photons. w_{stot} is used in tight P.I.D. criteria[9].

- ΔE_s — the energy difference between the second-highest and lowest strip between the first two maxima, sensitive to multi-peak showers. ΔE_s is used in tight P.I.D. criteria[9].

- $E_{\mathbf{ratio}}$ — the normalized energy difference between the leading and subleading maxima in the strip layer, helping identify merged or asymmetric showers. E_{ratio} is used in both medium and tight P.I.D. criteria[9].

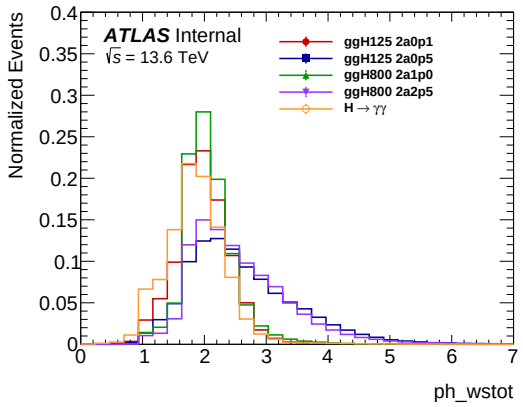

(a) (Shower Shape Variable w_{stot}, Normalized with four signals and $H \to \gamma\gamma$)

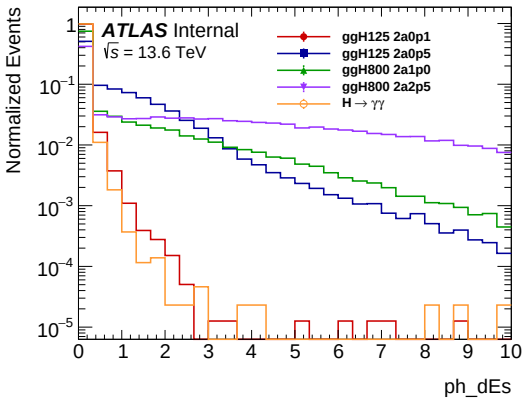

(b) (Shower Shape Variable ΔE_s, Normalized with four signals and $H \to \gamma\gamma$)

Figure 10: *Shower Shape Histograms for w_{stot} and ΔE_s*

Both w_{stot} and ΔE_s are variables included in the tight trigger selection criteria. From the distributions shown in Figure 10, it is evident that these variables vary significantly with ALP mass. In particular, the higher-mass ALP samples exhibit broader distributions relative to the $H \to \gamma\gamma$ reference, which likely contributes to the reduced trigger efficiencies observed for the tight trigger efficiencies at increased ALP masses.

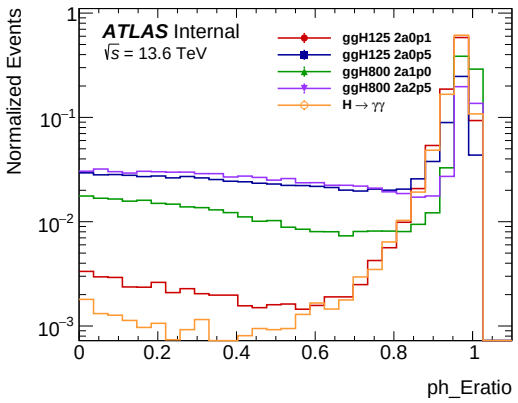

Figure 11: *(Shower Shape Variable E_{ratio}, Normalized with four signals and $H \to \gamma\gamma$)*

The variable $\mathbf{E}_{\text{ratio}}$, which is used in both the medium and tight trigger selection criteria, exhibits a noticeably broader distribution for higher-mass ALP signals. This behavior indicates that the photon jets become less collimated as the ALP mass increases, resulting in wider electromagnetic showers. This trend is consistent across all three shower shape variables analyzed (w_{stot}, ΔE_s, E_{ratio}) and provides a clear explanation for the declining trigger efficiencies observed with increasing ALP mass under the medium and tight working points.

4 Summary and Conclusions

This study investigated the efficiency of various diphoton triggers in detecting events consistent with the decay of a heavy scalar particle (X) into two Axion-Like Particles (ALPs), which subsequently decay into collimated photon pairs ($X \to aa \to \gamma\gamma\gamma\gamma$). Utilizing Monte Carlo simulations across a range of ALP masses, we observed that while loose trigger criteria generally maintain high efficiency across all ALP masses, medium and tight trigger efficiencies significantly degrade as the ALP mass increases.

Our analysis of shower shape variables (specifically w_{stot}, ΔE_s, and E_{ratio}) revealed that these variables exhibit broader distributions for higher ALP masses compared to the $H \to \gamma\gamma$ sample. This broadening indicates that the decay photons from heavier ALPs are less collimated, leading to wider electromagnetic showers in the ATLAS Liquid Argon (LAr) Calorimeter and making them more likely to be rejected by standard triggers. Since medium and tight trigger selections incorporate stricter criteria based on these shower shapes, the observed degradation in their efficiency is directly attributable to this increased non-collimation.

These findings highlight a critical challenge in searching for ALPs with higher masses at the LHC: the current medium and tight photon triggers, designed for more isolated photon signatures, may inadvertently suppress sensitivity to multi-photon final states from ALP decays due to the merging of highly collimated photons. Future efforts to optimize trigger strategies and develop machine learning algorithms capable of distinguishing merged photon signatures from background will be crucial for enhancing the sensitivity of ALP searches and other similar Beyond Standard Model phenomena.

5 Acknowledgements

I would like to extend my gratitude to the individuals and organizations who made this research possible. My deepest thanks go to Professor John Parsons, Dr. Lauren Osojnak, and Gabriel Matos for their invaluable guidance, mentorship, and support throughout this project. Their insights were instrumental in navigating this work.

I am also incredibly grateful to Professor Georgia Karagiorgi and Professor Reshmi Mukherjee for organizing the 2025 Nevis REU and making this opportunity possible. I also wish to express appreciation to Amy Garwood, who showed great care in managing the REU student's financial affairs, housing arrangements, and overall well-being.

This research greatly benefited from the resources and collaborative environment provided by The ATLAS Team. Their dedication to pushing the boundaries of particle physics is truly inspiring.

Finally, I gratefully acknowledge the financial support from The National Science Foundation (NSF). Without Grant No. PHY-2349438 this work would not have been possible.

References

[1] CERN. The standard model of particle physics, n.d.

[2] Anson Hook. Tasi lectures on the strong cp problem and axions, 2023.

[3] ATLAS Collaboration. Atlas open data: Experiment overview. n.d.

[4] Henric Wilkens and (on behalf of the ATLAS LArg Collaboration). The atlas liquid argon calorimeter: An overview. *Journal of Physics: Conference Series*, 160(1):012043, April 2009.

[5] G. Aad, E. Aakvaag, Et al. Abbott, and The ATLAS collaboration. The atlas trigger system for lhc run 3 and trigger performance in 2022. *Journal of Instrumentation*, 19(06):P06029, jun 2024.

[6] M. Aaboud, G. Aad, and Et al. Abbott. Search for pairs of highly collimated photon-jets in pp collisions at $\sqrt{s} = 13$ TeV with the atlas detector. *Phys. Rev. D*, 99:012008, Jan 2019.

[7] G. Aad, B. Abbott, and Et al. Abeling. Search for short- and long-lived axion-like particles in $h \to aa \to 4\gamma$ decays with the atlas experiment at the lhc. *The European Physical Journal C*, 84(7), July 2024.

[8] ATLAS Collaboration. Egamma identification run 2: Photon cleaning, n.d. CERN TWiki.

[9] G. Aad, Et al. Abbott, and The ATLAS collaboration. Electron and photon energy calibration with the atlas detector using lhc run 2 data. *Journal of Instrumentation*, 19(02):P02009, feb 2024.